Acta Chemica Scandinavica A 38 (1984) 1–13

Magnetic Behaviour of $Mn_{1-t}Cr_tAs$ ($0.20 < t < 0.40$)

HELMER FJELLVÅG and ARNE KJEKSHUS

Kjemisk Institutt, Universitetet i Oslo, Blindern, Oslo 3, Norway

The low temperature magnetic properties of $Mn_{1-t}Cr_tAs$ for $0.20<t<0.40$ have been re-examined by X-ray and neutron diffraction and differential scanning calorimetry. Double, helimagnetic arrangements with propagation vectors along the crystallographic *a* and/or *c* directions prevail in the co-operative magnetic state. As a unique feature for $Mn_{1-t}Cr_tAs$ among the MnP type phases, the H_a- and H_c-mode coexist (H_a being the low temperature variant) in a narrow composition range around $t=0.37$. Characteristic parameters for the two modes, such as the Neél temperature, the enthalpy change at the MnP,H to MnP,P type transition and the spiral propagation vector decrease monotonically towards $t=0.37$ (*viz.* both from above and below $t=0.37$).

A remarkable feature of the MnP type atomic arrangement is that it can accommodate a number of differently ordered magnetic structures, *viz.* a variety of ferro-(F), antiferro-(AF) and helimagnetic (H) modes depending on composition, temperature, pressure, external magnetic field, *etc.* However, the characteristic double H_a and H_c configurations (*cf.* Ref. 1) have apparently become almost a trademark for the MnP type family (at least for its magnetic frontage).

Table 1 gives an account of the binary compounds and ternary solid solution phases which take the MnP type chemical structure as well as the co-operative magnetic H_a- and/or H_c-mode. (A number of ternary, particularly phosphide, phases have recently been studied at this Institute, but since the results are yet unpublished they are not included in Table 1.) In view of the rather overwhelming amount of experimental data, the engagement on the theoretical aspects of these apparently interesting and unique findings is surprisingly scarce (*cf.* Refs. 18,21). The prototype itself, MnP, is by far the most thoroughly studied, and for this compound the contours of a theoretical framework have emerged (*cf.* Ref. 22 and references therein).

According to the number of representatives listed in Table 1 the H_c variant is far more

Table 1. Survey of MnP type phases which have been reported to adopt the (co-operative magnetic) H_a- and/or H_c-mode.

Helimagnetic sub-class	Binary representative	Ternary (solid solution) phase	
H_a		$Mn_{1-t}T_tAs$	T=V[2],Cr[3,4],Fe[1],Co[5],Ni[6]
		$MnAs_{1-x}X_x$	X=P[7,8]
H_c	MnP[9]	$Mn_{1-t}T_tP$	T=Fe[10]
	FeP[11]	$Fe_{1-t}T_tP$	T=Mn[10]
		$FeP_{1-x}X_x$	X=As[12]
	CrAs[13,14]	$Cr_{1-t}T_tAs$	T=V[15],Mn[3,4],Co[16],Ni[6]
		$CrAs_{1-x}X_x$	X=P[17],Sb[18]
	FeAs[19]	$Fe_{1-t}T_tAs$	T=Cr[20],Mn[1],Co[16]
		$FeAs_{1-x}X_x$	X=P[12]

0302-4377/84 $2.50

common than H_a, the latter variant being confined to $Mn_{1-t}T_tAs$, $MnAs_{1-x}X_x$ and probably MnAs when subjected to pressure.[23] Only three of the ternary phases can apparently accommodate both the H_a and H_c configurations (under the government of composition and temperature). For $Mn_{1-t}Fe_tAs$[1] and $MnAs_{1-x}P_x$[7,24] the H_a- and H_c-mode are separated by two-phase regions in the pseudo-binary phase diagrams. For $Mn_{1-t}Cr_tAs$, however, the available experimental data[3,4,25] suggest that the H_a- and H_c-mode may coincide in the composition range $0.35<t<0.40$.

The present study of $Mn_{1-t}Cr_tAs$ was undertaken in order to choose between the possibilities:

(i) magnetic transformation H_a to H_c (or *vice versa*) with temperature,

(ii) chemical and/or magnetic segregation into two phases.

In order to clarify this problem the composition range $0.20<t<0.40$ and temperature interval $10<T<\sim300$ K were re-examined.

EXPERIMENTAL

The pure elements used as starting materials for the syntheses were 99.999 % Cr-flakes (Koch-Light Laboratories Ltd.), 99.99 % Mn-flakes (Johnson, Matthey & Co. Ltd.) and 99.9999 % As-lumps (Koch-Light Laboratories Ltd.). According to earlier experience, equilibria in syntheses of ternary phases are most readily attained when preparations of the binary compounds are introduced as intermediate steps in the procedures.

The binary compounds MnAs and CrAs were prepared by heating stoichiometric quantities of the elements (ground powders of Cr- and Mn-flakes) in evacuated, sealed silica tubes. The temperature in the horizontally positioned furnaces was slowly increased (2×50 °C/d) to 900 °C for MnAs and 1000 °C for CrAs. After cooling to room temperature over 1 d the samples were crushed and subjected to one further heat treatment at 900 °C for 1 week, followed by cooling to room temperature over 1 d.

Ternary $Mn_{1-t}Cr_tAs$ samples were made similarly from the binary compounds. After a first heat treatment at 950 °C for 1 week, the samples were crushed and reheated at 700 °C for 3 weeks, and finally slowly cooled to room temperature over 1 d.

Room temperature X-ray powder diffraction photographs were taken in a Guinier camera ($CuK\alpha_1$ radiation, $\lambda=154.0598$ pm, Si[26] as internal standard, $a=543.1065$ pm). Unit cell dimensions were derived by applying the method of least squares (to the generally sharp, well-defined Guinier photographs).

Low temperature X-ray photographs were obtained between ~120 and ~300 K in an Enraf-Nonius (FR 553) Guinier-Simon camera ($CuK\alpha_1$ radiation, quartz crystal monochromizer, Si or Ag as internal standards). The samples were contained in sealed, thin-walled quartz capillaries. The temperature was regulated via a Pt resistance thermometer and a digital programmer synchronized the temperature with the movement of the film cassette. The difference between the programmed and actual temperature at the sample position reflects the thermal gradient between the sensor and the sample. The actual sample temperature is considered to be well within 2 K from the registered temperature.

The powder neutron diffraction data were collected with the OPUS II two-axis spectrometer between 10 K and room temperature. Cylindrical sample holders of vanadium were used. The temperature was controlled and regulated within ±0.5 K by a Thor (3010) controller (chromel/gold 0.07 % Fe thermocouple) connected to a Displex cooling system. Neutrons of wavelength 187.7 pm were obtained from the Kjeller reactor JEEP II. The nuclear scattering lengths (in 10^{-12} cm) $b_{Cr}=0.353$, $b_{Mn}=-0.370$ and $b_{As}=0.64$ were taken from Ref. 27. The magnetic formfactor for Mn^{3+} was taken from Ref. 28. The Hewat[29] version of the profile refinement programme by Rietveld[30] was applied in the final fitting of the variable parameters.

The helimagnetic parameters were derived from the intensities of the appropriate reflections by the programme SPIRAL.[31]

Magnetic susceptibilities were measured between 80 and 1000 K by the Faraday method (maximum field ~8 kOe using 10–15 mg samples).

Low temperature differential scanning calorimetry (DSC) measurements were performed with a Mettler TA 3000 system consisting of a TG10 TA processor and a DSC30 cell. Samples of ~100 mg were used, the heating rate was 10 K/min and the temperature range ~100–~500 K was covered. Data reduction and evaluation of thermodynamic parameters were performed with standard programmes for the system.

CRYSTAL STRUCTURE DATA

Although the principal aim of this study has been to elucidate the low temperature magnetic properties of $Mn_{1-t}Cr_tAs$, various other experimental data have come to hand as by-products.

In complete accordance with Ref. 3, $Mn_{1-t}Cr_tAs$ with $0.20 \leqq t \leqq 0.40$ takes the MnP type atomic arrangement at, and below, room temperature. Since the Bragg reflections are generally sharp and no additional super-structure reflections were observed, the substituted atoms appear to be randomly distributed over the metal sub-lattice (as seen by the X-ray and neutron diffraction techniques). The unit cell dimensions and positional parameters (as derived from powder neutron diffraction data) given in Table 2, fall in quite well with the corresponding data in Ref. 3. The room temperature unit cell dimensions *versus* the compositional parameter t for the additional small scale samples of $Mn_{1-t}Cr_tAs$ (Fig. 1) also matches the corresponding data in Ref. 3. (The few, negligible distinctions that nevertheless occur are easily attributed to sample quality and data handling in the present study or methodological differences between X-ray and neutron diffraction.)

When judging or using the data in Table 2 it should be remembered that the positional parameters for the metal atoms are burdened with relatively large uncertainties due to their small effective scattering lengths. An additional structure refinement complication stems from the marked overlapping of reflections which occurs when c/b approximates $\sqrt{3}$ for certain compositions (most pronounced for $t=0.39$) and temperatures.

The conical perturbation of the H_a-mode reported for $0.25 \leqq t \leqq 0.35$ in Ref. 3, represents a

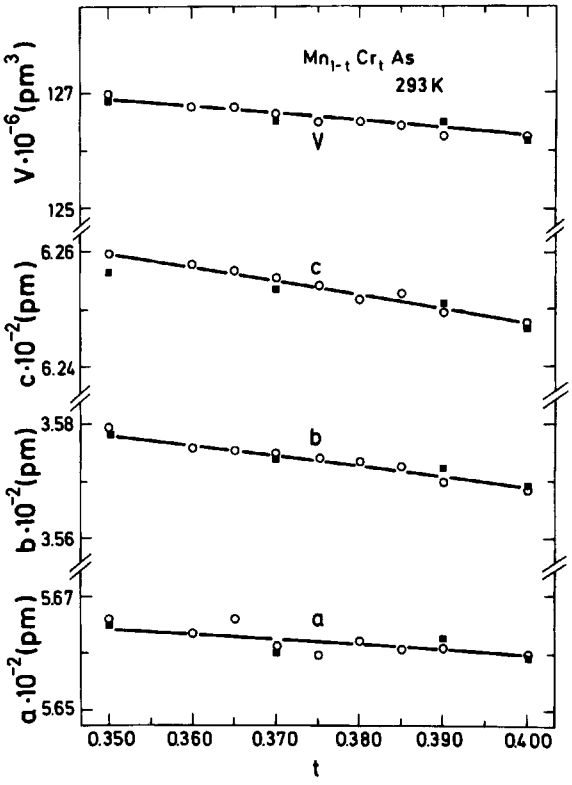

Fig. 1. Room temperature unit cell dimensions of $Mn_{1-t}Cr_tAs$ ($0.35 \leqq t \leqq 0.40$). Error limits do not exceed twice the size of symbol. Circles and squares represent results derived from X-ray and neutron diffraction data, respectively. (1 Å$=10^2$ pm.)

a

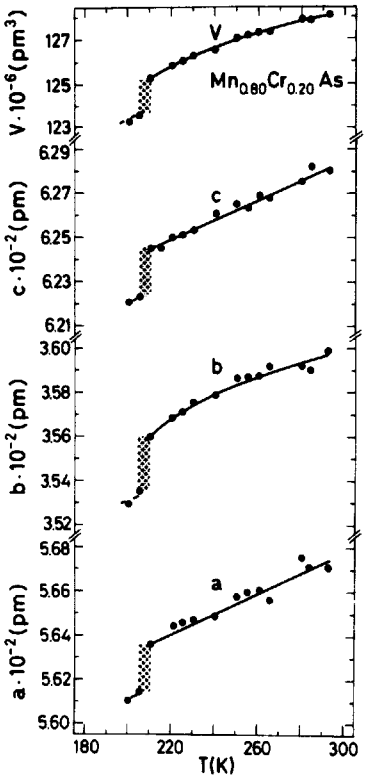
Mn0.80Cr0.20As
V·10⁻⁶(pm³)
c·10⁻²(pm)
b·10⁻²(pm)
a·10⁻²(pm)
T(K)

b

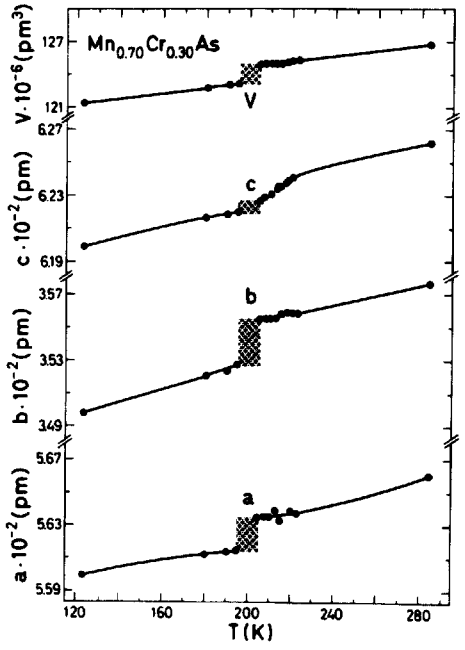
Mn0.70Cr0.30As
V·10⁻⁶(pm³)
c·10⁻²(pm)
b·10⁻²(pm)
a·10⁻²(pm)
T(K)

c

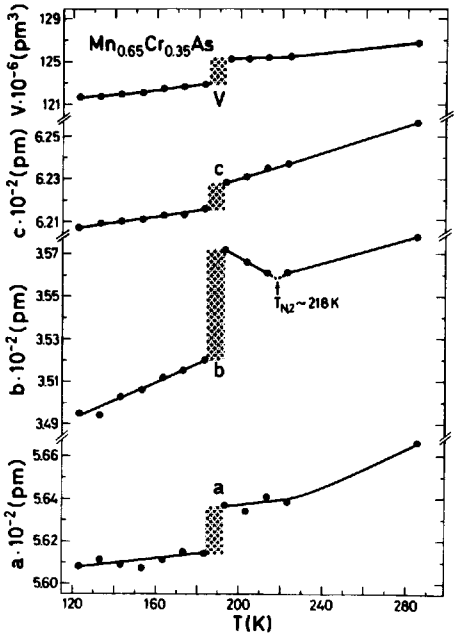
Mn0.65Cr0.35As
V·10⁻⁶(pm³)
c·10⁻²(pm)
b·10⁻²(pm)
a·10⁻²(pm)
T(K)
T_N2~218K

d

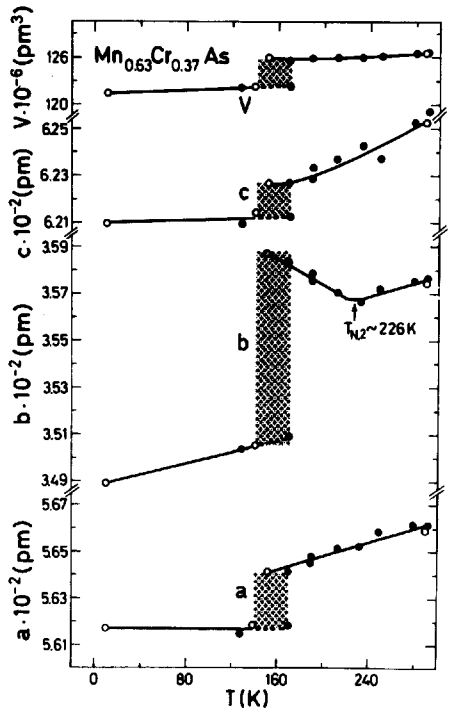
Mn0.63Cr0.37As
V·10⁻⁶(pm³)
c·10⁻²(pm)
b·10⁻²(pm)
a·10⁻²(pm)
T(K)
T_N2~226K

e

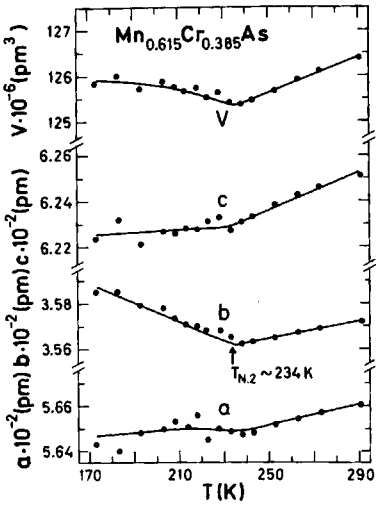

Fig. 2. Unit cell dimensions *versus* temperature for selected samples of $Mn_{1-t}Cr_tAs$ at temperatures below 300 K; (a) $Mn_{0.80}Cr_{0.20}As$, (b) $Mn_{0.70}Cr_{0.30}As$, (c) $Mn_{0.65}Cr_{0.35}As$, (d) $Mn_{0.63}Cr_{0.37}As$, and (e) $Mn_{0.615}Cr_{0.385}As$. Error limits do not exceed the size of symbols. Filled and open circles represent results derived from X-ray and neutron diffraction data, respectively. (1 Å=10^2 pm.) $T_{N.2}$ refers to temperature of the MnP,H_c ⇄ MnP,P type transition. Shaded regions refer to two-phase regions between MnP,H_a and MnP,P type states (for $Mn_{0.80}Cr_{0.20}As$ and $Mn_{0.70}Cr_{0.30}As$) or between MnP,H_a and MnP,H_c type states (for $Mn_{0.65}Cr_{0.35}As$ and $Mn_{0.63}Cr_{0.37}As$).

further problem since ferromagnetic parameters generally interfere with positional parameters in the least squares refinement procedure. For this reason the structural data for $Mn_{1-t}Cr_tAs$ derived by the powder neutron diffraction technique are bound to be burdened with large uncertainties. In view of the need for structural information for model considerations, attempts will now be made to activate low temperature X-ray methods (for powders or, since promising openings for crystal growths have come to hand, hopefully also for single crystals).

The variations in the unit cell dimensions of $Mn_{1-t}Cr_tAs$ for t=0.20, 0.30, 0.35, 0.37 and 0.385 with temperature are shown in Fig. 2. One or more phase transformations are distinctly reflected in these curves. The hysteresis accompanied, first order transitions for t=0.20, 0.30,

Table 2. Unit cell dimensions and positional parameters with standard deviations for some $Mn_{1-t}Cr_tAs$ samples as derived by Rietveld analysis of neutron diffraction data. Space group *Pnma*; Mn/Cr in 4*c* and As in 4*c*. (Nuclear R_n-factors ranging between 0.04 and 0.05, profile R_p-factors ranging between 0.11 and 0.13; 28–30 nuclear reflections.)

t	T(K)	a(pm)	b(pm)	c(pm)	c/b	x_T	z_T	x_X	z_X
0.25	295	566.46(5)	358.65(4)	626.43(8)	1.7466	0.012(8)	0.219(8)	0.210(1)	0.578(1)
	10	558.41(6)	348.65(5)	617.60(9)	1.7714	0.009(8)	0.209(8)	0.200(1)	0.579(1)
0.37	295	565.97(5)	357.37(4)	625.30(9)	1.7497	0.021(8)	0.218(8)	0.209(1)	0.579(1)
	140	561.77(9)	350.51(5)	621.50(12)	1.7731	0.004(8)	0.209(6)	0.202(1)	0.582(1)
	10	561.60(9)	348.85(5)	621.09(11)	1.7803	0.016(8)	0.203(5)	0.203(1)	0.578(1)
0.39	295	566.30(5)	357.28(5)	625.09(9)	1.7491	0.002(10)	0.192(7)	0.210(1)	0.579(2)
	175	564.40(6)	358.97(16)	621.85(27)	1.7323	0.015(12)	0.185(10)	0.210(1)	0.580(4)
	10	563.43(6)	359.54(16)	621.34(28)	1.7282	0.010(15)	0.189(10)	0.209(1)	0.576(4)

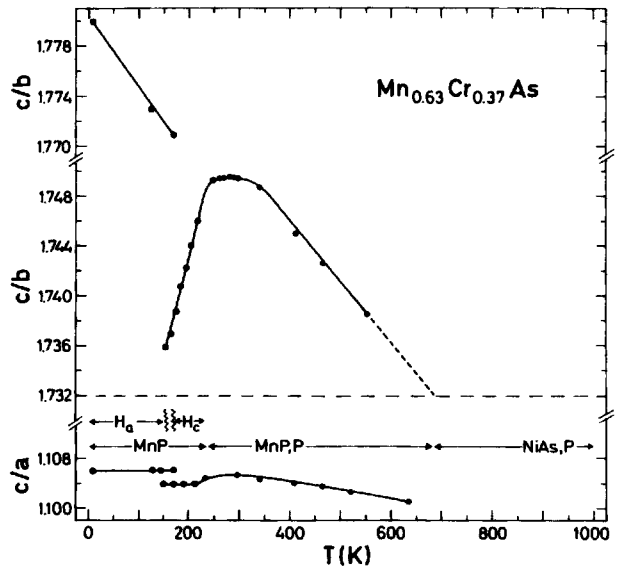

Fig. 3. Axial ratios *c/a* and *c/b versus* temperature for $Mn_{0.63}Cr_{0.37}As$. Dashed line corresponds to the ideal orthohexagonal ratio $c/b \equiv \sqrt{3}$.

0.35 and 0.37 [Fig. 2 (a)–(d)] where the hysteresis loop increases in the said order, represent the most prominent feature in this picture.

The thermal expansion curves for t=0.35, 0.37 and 0.385 also show sign of a second (or higher) order phase transition through a marked change in slope of *b versus* temperature. As may be expected from the data in Fig. 2 the axial ratios *c/a* and *c/b* demonstrate peculiar and interesting temperature dependences and the results for $Mn_{0.63}Cr_{0.37}As$ (Fig. 3) can serve as an example. When *c/b* obtains the value $\sqrt{3}$ at higher temperatures this is merely a manifestation of that the MnP⇄NiAs type transition has taken place (*cf.* Refs. 3,25,32). The fact that $Mn_{1-t}Cr_tAs$ also takes $c/b \approx \sqrt{3}$ at lower temperature is accidental in the sense that the MnP type atomic arrangement is retained. This again demonstrates that little significance should be attached to the axial ratio alone as a structure determining criterion.

PHASE DIAGRAM DATA

A section of the phase diagram for MnAs–CrAs is presented in Fig. 4. The diagram is constructed on the basis of the structural data considered in the preceeding section together with magnetic and thermo-analytical DSC data outlined in succeeding sections.

The widths of the hysteresis regions in Fig. 4 correspond to temperature intervals hatched on Fig. 2 (a)–(d). As seen on comparing Figs. 2(e) and 4, the sample with t=0.385 is considered to be a borderline case which just escapes the hysteresis accompanied, first order transition.

As indicated on the inset illustration in Fig. 4 all transitions are believed to be of magnetic origin. Apart from the question of conical spiral deformation, which is left open in this study, the phase diagram in Fig. 4 is merely a detailed version of the relevant section of the phase diagram given in Ref. 3, where also comments to the phase diagram of Kazama and Watanabe[25] are found. Fig. 4 is, on the other hand, distinctly different from the magnetic phase diagram proposed in Ref. 4. The distinction is probably less pronounced than at first sight, and may be mainly a consequence of the external field applied in the study of Wöhl *et al.*[4]

For t=0.20 and 0.30 the transition occurs between the MnP,H_a and MnP,P type states at the temperature denoted $T_{N,1}$. This transition was earlier considered to be of the continuous second (or higher) order type in $Mn_{1-t}Cr_tAs$ (in

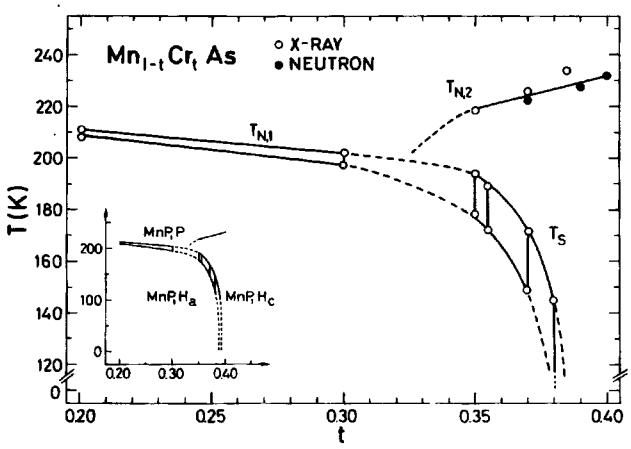

Fig. 4. Magnetic phase diagram for $Mn_{1-t}Cr_tAs$ ($0.20 \leqq t \leqq 0.40$). The bars represent the width of hysteresis as determined by X-ray diffraction.

line with findings for the corresponding $Mn_{1-t}T_tAs$ listed in Table 1). On careful examination, this study, however, reveals that the discontinuous feature of the transition is quite distinct. Whether or not the same applies to the other $Mn_{1-t}T_tAs$ phases remains an open question.

A hysteresis accompanied transition is also observed for t=0.35, 0.355, 0.37 and 0.38. Although this transition manifests itself in the low temperature X-ray and DSC data similarly to the transition described for t=0.20 and 0.30, examination by neutron diffraction reveals that it is of the MnP,H_a to MnP,H_c type (see inset to Fig. 4). Despite the difference in magnetic nature of the latter transition (denoted T_S) it appears as a continuation of $T_{N,1}$ in Fig. 4. However, the details of the phase diagram are not well established in the region between t=0.30 and 0.35. In this composition range the three curves $T_{N,1}$, $T_{N,2}$ and T_S probably meet in a triple point.

In addition, the samples t=0.35, 0.355, 0.37 and 0.38, undergo another, second (or higher) order, transition at the somewhat higher temperature $T_{N,2}$. According to neutron diffraction this transition is of the MnP,H_c $\rightleftharpoons$ MnP,P type. Only this latter transition is observed in the samples t=0.385, 0.39 and 0.40. The MnP,H_c $\rightleftharpoons$ MnP,P type transition is reflected in the inflection point of the thermal expansion curves for the *b*-axis [Fig. 2 (c)–(e)]. This phenomenon is probably a

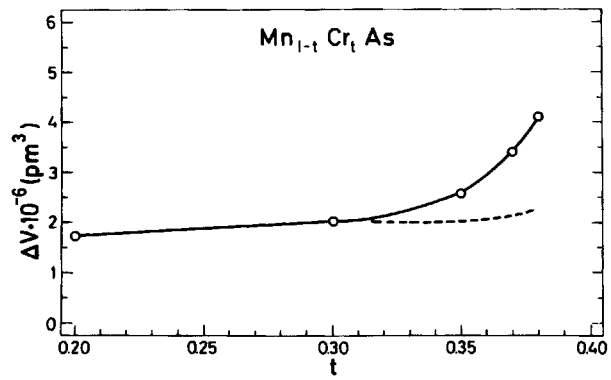

Fig. 5. Change in unit cell volume at the MnP,H_a to MnP,P type transition (for $t \leqq 0.30$) or MnP,H_a to MnP,H_c type transition (for $t \geqq 0.35$). (1 Å=10^2 pm.) Broken curve see text.

Table 3. Characteristics of helimagnetic modes in MnP type phases (*cf.*, *e.g.*, Refs. 1,3,7,9).

Property	H_a-mode	H_c-mode
Magnetic unit cell	Incommensurate magnetic arrangement based on chemical unit cell (*Pnma*)	
Numbering of magnetic atoms	$(1)x_{4,z};(2)\bar{x}_{4,\bar{z}};(3)\frac{1}{2}-x_{4,\frac{1}{2}}+z;(4)\frac{1}{2}+x_{4,\frac{1}{2}}-z$	
Spiral propagation	Parallel to a [$\tau=(\tau_a,0,0)$]	Parallel to c [$\tau=(0,0,\tau_c)$]
Extinction rules for helimagnetic reflections	$hk0$ absent when $h=2n+1$	$0kl$ absent when $k+l=2n+1$
Moment orientation	In bc-plane	In ab-plane
Phase relations for spirals (Index refers to atom No.)	$\phi_1=\phi_4\neq\phi_2=\phi_3$	$\phi_1=\phi_3\neq\phi_2=\phi_4$
Chemical dependence of phase difference $\phi_{1,2}$ ($=\phi_2-\phi_1$)	Relatively independent on T,t,X,x $25<\phi_{1,2}<105°$	Strongly dependent on chemical composition
Temperature dependence of $\phi_{1,2}$	Increasing $\phi_{1,2}$ with increasing T/T_N	Almost independent of T/T_N
Chemical dependence of periodicity $\lvert\tau\rvert^{-1}$	$4.8<\lvert\tau\rvert^{-1}<16.1$ at 10 K Usually increasing with t (except for T=Co)	$2.2<\lvert\tau\rvert^{-1}<10.0$ at 10 K Strongly dependent on chemical composition
Temperature dependence of $\lvert\tau\rvert^{-1}$	Decreasing $\lvert\tau\rvert^{-1}$ with increasing T/T_N	Dependent on chemical composition

magnetostrictive effect, which appears to be a general feature for the MnP,H_c to MnP,P type transition.

The discontinuous change in the unit cell volume ($\Delta V=V_2-V_1$; $T_2>T_1$) at the first order transition varies with the compositional parameter t as shown by the solid curve in Fig. 5. ΔV is seen to increase by a factor ~2 between t=0.30 and 0.38. However, this substantial increase is closely connected with:

(i) The occurrence of the H_c-mode with its unusual thermal expansion properties for the unit cell volume (*cf.* Fig. 2),

(ii) The temperature span of the H_c-mode varies appreciably with t (*cf.* Fig. 4).

When ΔV is corrected for the combined effect of these factors the broken curve in Fig. 5 is obtained, and the compositional dependence of the corrected ΔV has become almost negligible.

Another feature which seems worth noting is that ΔV at the first order, co-operative to paramagnetic transition is positive ($\Delta V\approx+2\times10^6$ pm^3) in $Mn_{1-t}Cr_tAs$ ($0.20\geqq t\geqq0.30$) as opposed to its binary end members MnAs ($\Delta V\approx-3\times10^6$ pm^3) and CrAs ($\Delta V\approx-2.5\times10^6$ pm^3).

HELIMAGNETIC STRUCTURES

Characteristic features of the helimagnetic structures in MnP type phases are summarized in Table 3. In this study experimental data have been collected for samples with t=0.25, 0.37 and 0.39. $Mn_{0.75}Cr_{0.25}As$ was studied mainly to clarify whether the magnetic transition is accompanied with a hysteresis or not. On the other hand, the samples with t=0.37 and 0.39 are both in the composition range where coexistence of the H_a- and H_c-modes is expected.

As evident from Table 3 the two helimagnetic modes have many features in common. However, the systematic absences for the satellite reflections in the neutron diffraction patterns facilitate an unambiguous determination of the mode present in each case.

The magnetic reflections could be indexed as required by an H_a-mode for t=0.25 and 0.37 for $T<T_S$ and as an H_c-mode for t=0.37 for $T_S<T<T_{N,2}$ and t=0.39 for $T<T_{N,2}$. (Numerical values for the temperatures are: $T_{N,1}$=203−207 K for t=0.25 and T_S=150−175 K for t=0.37; $T_{N,2}$=223±2 K and 228±2 K for t=0.37 and 0.39,

Table 4. Helimagnetic parameters for $Mn_{1-t}Cr_tAs$. (R_{spiral} ranging between 0.05 and 0.09; 6–7 magnetic satellite reflections.)

t	0.37			0.39	
T(K)	10	140	150	10	175
$\tau_a/2\pi a^*$	0.062(4)	0.073(4)			
$\tau_c/2\pi c^*$			0.242(3)	0.251(2)	0.252(2)
$\mu_H(\mu_B)$	1.84(10)	1.45(10)	1.30(10)	1.89(10)	1.45(10)
$\phi_{1,2;a}(°)$	39(10)	46(10)			
$\phi_{1,2;c}(°)$			−147(10)	−152(5)	−145(10)
T_S (K)	175(3)[a]				
$T_{N,2}$(K)	223(3)			228(3)	

[a] Upon heating.

respectively.) The spiral parameters μ_H and $\phi_{1,2}$ (see Table 3) were deduced from the best fit as judged from the reliability factor $R_{spiral}= \Sigma|I_i(obs)-s\cdot I_i(calc)|/\Sigma I_i(obs)$.

The spiral parameter β[13] was fixed at 90° in all calculations. The possibility of magnetic contributions to the Bragg (nuclear) reflections could not be established with certainty. A ferromagnetic component along *a* would be consistent with deductions in Refs. 3,4,25, and this assumption led in fact to somewhat lower reliability factors in some of the structural refinements (see the section on crystal structure data). Single crystal neutron diffraction and/or polarized neutron analysis could resolve this question.

The results given in Table 4 are generally in agreement with the data presented in Ref. 3. The numerical values for $\phi_{1,2}$ for the H_c-mode are indeed somewhat larger than the corresponding values in Refs. 3,13. However, the error limits are easily underestimated due to the fact that the satellite intensities are generally low and superimposed on a fluctuating background.

The transition between the H_a- and H_c-mode in $Mn_{0.63}Cr_{0.37}As$ is clearly demonstrated in Fig. 6 which shows how the integrated intensity of the well resolved $000^{\pm}$ satellites for the two modes change with temperature. This magnetic phase transition is directly coupled to the first order structural phase transition described earlier. The width of the hysteresis region for the magnetic transition determined by neutron diffraction complies well with the temperature range determined from X-ray diffraction for the chemical

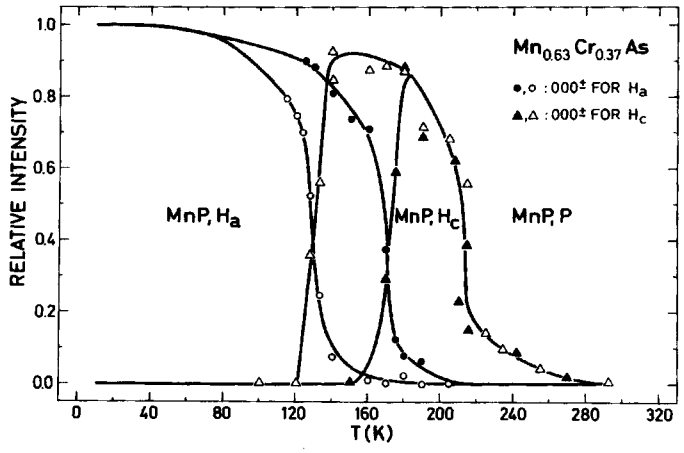

Fig. 6. Relative intensities of $000^{\pm}$ for the H_a- and H_c-mode *versus* temperature. Open and filled symbols refer to data obtained upon cooling and heating, respectively.

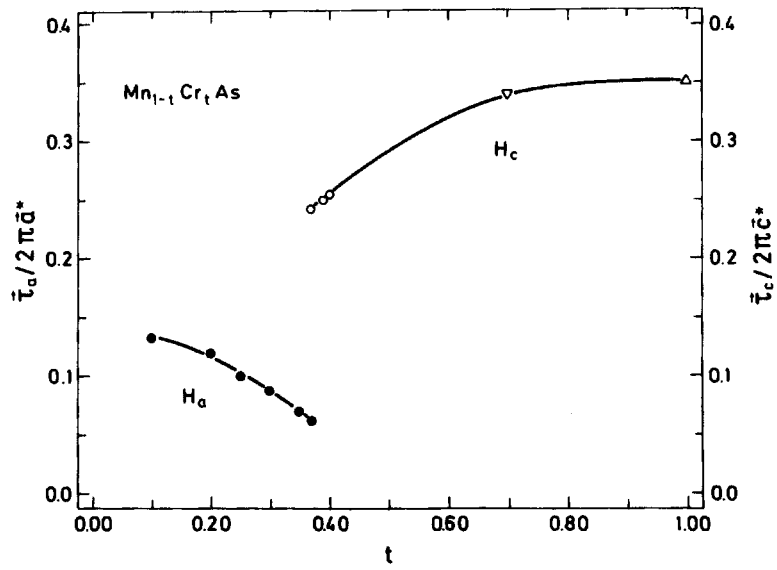

Fig. 7. Variation of the component τ_a or τ_c of the propagation vectors with t at 10 K. Data for $t=1.00$ taken from Ref. 13 and for $t=0.70$ (temperature not specified) from Ref. 25.

transition (*cf.* preceeding section). Repeated measurements showed that the equilibrium condition is reasonably well established in the examination of the MnP,H_a to MnP,H_c type transition. The sigmoidal shape of the hysteresis loop curves may to some extent be attributed to the inevitable minute concentration variations within the large scale neutron diffraction samples.

Fig. 7 shows the composition dependence of the propagation vectors ($\tau_a/2\pi a^*$ or $\tau_c/2\pi c^*$) at 10 K. The value of $\tau_c/2\pi c^*$ for $t=0.37$ refers to 150 K, but in this composition range (*cf.* Table 4) $\tau_c/2\pi c^*$ varies only slightly with temperature. It is worthwhile to denote that both propagation vectors decrease towards $t=0.37$, and in this respect Fig. 7 shows some resemblence to Fig. 4. In addition to the change in propagation direction, there is also a discontinuous shift in the magnitude of the propagation vector at the MnP,H_a to MnP,H_c type transition (see Table 4, Fig. 7 and Ref. 3). The transition has a similar effect on $\phi_{1,2}$, whereas the magnetic moment μ_H is maintained essentially unaltered through the transition. As emphasized above, $\phi_{1,2}$ is hampered with larger inaccuracy, but at least for the H_a-mode its composition dependence follows the same trend as for the propagation vector.

The present study has unequivocally showed that the H_a- and H_c-mode occur as low and high temperature variants, respectively, in a composition range around $t=0.37$. This is the first evidence for this type of co-operative magnetic coexistence for the MnP type phases, but similar phenomena are well known for other phases (*cf.*, *e.g.*, Refs. 33,34). The stability conditions for the H_a- and H_c-mode have been examined by the group theoretical Bertaut method.[18,35] However, while the stability conditions for the H_c-mode could be derived[18] on the basis of isotropic exchange interactions, the account for the H_a-mode required[35] a far more sophisticated exchange mechanism. Hence, the relative stability of two modes is not established.

MAGNETIC SUSCEPTIBILITY

Thermomagnetic curves for $Mn_{1-t}Cr_tAs$ samples with $0.10 \leqq t \leqq 0.60$ are shown in Fig. 8. (They were recorded primarily as a means to characterize the present samples.)

Starting from the high temperature side, the linear sections reflect the NiAs,P type state with defined values of μ_P and θ (μ_P ranging between 3.9 ± 0.3 and 4.5 ± 0.2 μ_B, θ ranging between

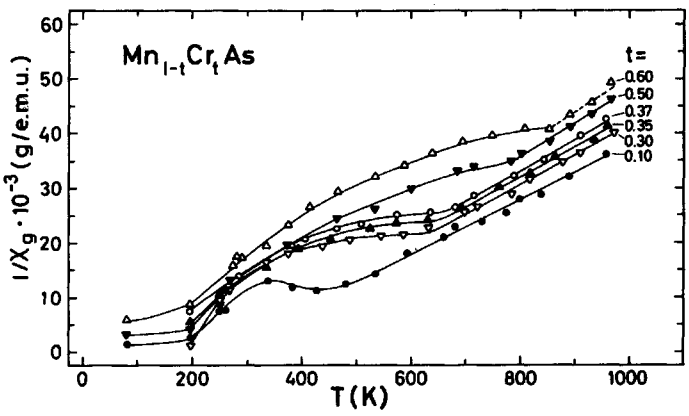

Fig. 8. Reciprocal magnetic susceptibility *versus* temperature for selected samples of $Mn_{1-t}Cr_tAs$.

225±25 and 250±10 K, as compared with μ_P=4.5±0.1 μ_B and θ=270±10 K for MnAs). In the intermediate section of the χ^{-1}(T) curves the MnP,P type state prevails, where the curve shape is influenced by the gradual reduction from a "high" to a "low" spin state, which in turn is related to how far the MnP type conversion has progressed (*cf.* Ref. 36). The low temperature section of the curves corresponds to the co-operative magnetic state.

TRANSFORMATION ENTHALPIES

In order to obtain an estimate of the energy quantities involved in the MnP,H_a to MnP,P, MnP,H_a to MnP,H_c and MnP,H_c $\rightleftharpoons$ MnP,P type transformations, DSC data were collected for various $Mn_{1-t}Cr_tAs$ samples. The results are summarized in Table 5, which also gives the transformation temperatures (upon heating) obtained by the X-ray and neutron diffraction techniques as well as literature values for the transformation enthalpies and temperatures for MnAs and CrAs. The transformation temperatures found by the different methods are generally in good agreement (Table 5).

The transformation enthalpies show a consistent trend with the compositional parameter t (Fig. 9). At first sight, it is somewhat remarkable that MnAs, which undergoes the NiAs,F to MnP,P type transition, fits the data for the MnP,H_a to MnP,P type transition. However, the

Table 5. Transition temperatures (peak positions for DSC; for X-ray and ND see text) and integrated enthalpies for $Mn_{1-t}Cr_tAs$[a] (on heating).

t	$T_{N,1}$ or T_S(K) DSC	X-ray	ND	ΔH(J/g)	$T_{N,2}$(K) DSC	X-ray	ND	ΔH(J/g)
0.20	212	211	208[c]	8.5				
0.30	204	202	202[c]	5.1				
0.35	186	194	195[c]	2.2		218		
0.36	182	185		1.9	217			0.3
0.37	167	172	175	1.3	222	226	223	1.0
0.38		145			227			2.0
0.39					234	230	228	2.1
1.00[b]					261			

[a] For t=0.00, T_C (NiAs,F to MnP,P)=318.6 K (DSC), 315 K (X-ray), 317 K (ND) and ΔH=15.6 J/g (literature: 315 K, 21.0 J/g[37,39]; 315.6 K, 25.2 J/g[37]; 318 K[40]) [b] For t=1.00, literature values for T_N and ΔH are: 259.86 K, 5.84 J/g[38]; 265 K, 4.09 J/g[41]; 272 K[13]; 280 K[42]. [c] Quoted from Ref. 3.

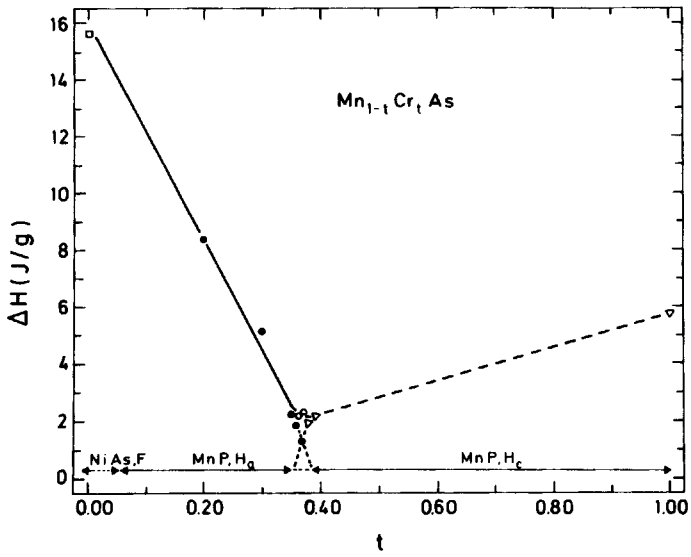

Fig. 9. ΔH *versus* t for $Mn_{1-t}Ct_tAs$. Square represents the NiAs,F to MnP,P type transition, filled circles the MnP,H_a to MnP,H_c or the MnP,H_a to MnP,P type transition, open circles the sum of the transition enthalpies for the MnP,H_a to MnP,H_c and MnP,H_c ⇄ MnP,P type transitions, while triangles represent values for the MnP,H_c ⇄ MnP,P type transition (first order for CrAs).

essential point is that the transitions take place between co-operative- and paramagnetic states. On the other hand, attention should be paid to the fact that the literature (*cf.* Ref. 37) gives scattered values for ΔH for the NiAs,F to MnP,P type transition in MnAs.

Contrary to the findings for MnAs the present ΔH value for the MnP,H_c to MnP,P type transition in CrAs concurs with that published by Blachnik *et al.*[38] In view of this somewhat conflicting situation for MnAs and CrAs it is not appropriate to suggest a general scaling of the present ΔH values.

The ΔH *versus* t relationship shows a distinct minimum around t=0.37, *i.e.* just the composition region where both the H_a- and H_c-mode coexist depending on temperature. In the composition range where both modes are found, the individual ΔH values for the MnP,H_a to MnP,H_c and MnP,H_c to MnP,P type transitions approach zero, and it is the sum of these contributions that constitutes the minimum.

Acknowledgement. This work has received financial support from The Norwegian Research Council for Science and the Humanities.

REFERENCES

1. Selte, K., Kjekshus, A. and Andresen, A. F. *Acta Chem. Scand. A 28* (1974) 61.
2. Selte, K., Kjekshus, A., Valde, G. and Andresen, A. F. *Acta Chem. Scand. A 30* (1976) 8.
3. Selte, K., Kjekshus, A., Peterzéns, P. G. and Andresen, A. F. *Acta Chem. Scand. A 32* (1978) 653.
4. Wöhl, R., Berg, H. and Bärner, K. *Phys. Stat. Sol. A 57* (1980) 179.
5. Selte, K., Kjekshus, A., Valde, G. and Andresen, A. F. *Acta Chem. Scand. A 30* (1976) 468.
6. Delphin, I. L. A., Selte, K., Kjekshus, A. and Andresen, A. F. *Acta Chem. Scand. A 32* (1978) 179.
7. Haneda, S., Kazama, N., Yamaguchi, Y. and Watanabe, H. *J. Phys. Soc. Jpn. 42* (1977) 1212.
8. Andresen, A. F., Fjellvåg, H., Skjeltorp, A. and Bärner, K. *AIP Conf. Proc. 89* (1981) 324.
9. Forsyth, J. B., Pickart, S. J. and Brown, P. J. *Proc. Phys. Soc. 88* (1966) 333.
10. Roger, A. and Fruchart, R. *C. R. Acad. Sci. C 264* (1967) 508.
11. Felcher, G. P., Smith, F. A., Bellavance, D. and Wold, A. *Phys. Rev. B 3* (1971) 3046.

12. Selte, K., Kjekshus, A., Oftedal, T. A. and Andresen, A. F. *Acta Chem. Scand. A 28* (1974) 957.
13. Selte, K., Kjekshus, A., Jamison, W. E., Andresen, A. F. and Engebretsen, J. E. *Acta Chem. Scand. 25* (1971) 1703.
14. Boller, H. and Kallel, A. *Solid State Commun. 9* (1971) 1699.
15. Selte, K., Hjersing, H., Kjekshus, A. and Andresen, A. F. *Acta Chem. Scand. A 29* (1975) 312.
16. Selte, K., Kjekshus, A., Aaby, S. and Andresen, A. F. *Acta Chem. Scand. A 29* (1975) 810.
17. Selte, K., Hjersing, H., Kjekshus, A., Andresen, A. F. and Fischer, P. *Acta Chem. Scand. A 29* (1975) 695.
18. Kallel, A., Boller, H. and Bertaut, E. F. *J. Phys. Chem. Solids 35* (1974) 1139.
19. Selte, K., Kjekshus, A. and Andresen, A. F. *Acta Chem. Scand. 26* (1972) 3101.
20. Selte, K., Fjellvåg, H., Kjekshus, A. and Andresen, A. F. *Acta Chem. Scand. A 33* (1979) 727.
21. Menyuk, N., Kafalas, J. A., Dwight, K. and Goodenough, J. B. *Phys. Rev. 177* (1969) 942.
22. Shapira, Y., Becerra, C. C., Oliveira, N. F. and Chang, T. S. *Phys. Rev. B 24* (1981) 2780.
23. Yoshie, H. and Hihara, T. *J. Phys. Soc. Jpn., 40* (1976) 427.
24. Roger, A. and Fruchart, R. *Mat. Res. Bull. 3* (1968) 253.
25. Kazama, N. and Watanabe, H. *J. Phys. Soc. Jpn. 30* (1971) 1319.
26. Deslatters, R. D. and Henins, A. *Phys. Rev. Lett. 31* (1973) 972.
27. *The Neutron Diffraction Commission,* 1976.
28. Watson, R. E. and Freeman, A. J. *Acta Crystallogr. 14* (1961) 27.
29. Hewat, A. W. The Rietveld Computer Program for the Profile Refinement of Neutron Diffraction Powder Patterns Modified for Anisotropic Thermal Vibrations, UKAERE Harwell Report RRL 73/897 (1973).
30. Rietveld, H. M. *J. Appl. Crystallogr. 2* (1969) 65.
31. Engebretsen, J. E. Computer Programmes for Elastic Scattering of Neutrons from Crystalline Powders, IFA, Kjeller 1970.
32. Franzen, H. F., Haas, C. and Jellinek, F. *Phys. Rev. B 10* (1974) 1248.
33. Burlet, P. and Bertaut, E. F. *J. Phys. Chem. Solids 30* (1969) 851.
34. Wong, P., Horn, P. M., Birgeneau, R. J. and Shirane, G. *Phys. Rev. B 27* (1983) 428.
35. Gribanov, I. F. and Zavadskii, E. A. *J. Magn. Magn. Mater. 37* (1983) 51.
36. Selte, K. and Kjekshus, A. *Acta Chem. Scand. 27* (1973) 3195.
37. Grønvold, F., Snildal, S. and Westrum, E. F. *Acta Chem. Scand. 24* (1970) 285.
38. Blachnik, R., Kudermann, G., Grønvold, F., Alles, A., Falk, B. and Westrum, E. F. *J. Chem. Thermodynamics 10* (1978) 507.
39. Bates, L. F. *Proc. Roy. Soc. (London) A 117* (1927) 680.
40. Basinski, Z. S., Kornelsen, R. O. and Pearson, W. B. *Trans. Indian Inst. Met. 13* (1960) 141.
41. Kazama, N. and Watanabe, H. *J. Phys. Soc. Jpn. 31* (1971) 943.
42. Watanabe, H., Kazama, N., Yamaguchi, Y., and Ohashi, M. *J. Appl. Phys. 40* (1969) 1128.

Received June 8, 1983.